Hindawi
Laser and Particle Beams
Volume 2022, Article ID 3740391, 11 pages
https://doi.org/10.1155/2022/3740391

Research Article

Study on Damage Characteristics of Fused Silica under Ion Beam Sputtering and AMP Technique

Wanli Zhang, Feng Shi, Ci Song, Ye Tian, and Shuangpeng Guo

Laboratory of Science and Technology on Integrated Logistics Support, College of Intelligence Science and Technology, National University of Defense Technology, Changsha, Hunan Province 410073, China

Correspondence should be addressed to Feng Shi; shifeng@nudt.edu.cn

Received 21 April 2022; Revised 17 June 2022; Accepted 22 June 2022; Published 27 September 2022

Academic Editor: Daniele Margarone

Fused silica is an optical material with excellent performance, and it is widely used in the fabrication of optics in various high-power laser systems. With the gradual improvement of laser systems, the quality of optics becomes crucial. Taking magnetorheological finishing (MRF), ion beam sputtering etching (IBSE), and advanced mitigation processing (AMP) as the means, this work focuses on exploring the damage characteristics evolution of fused silica under different techniques. In this work, IBSE technique was used to determinedly polish the optical surface after removing damage layer by MRF technique, and AMP technique was applied to etch the surface with a certain depth. Then, 10 J/cm^2 (355 nm, 5 ns) laser was used to irradiate the optical surface, and the damage density of optics maintained at a low level, about 0.001/mm^2, which proves that MRF, IBSE, and AMP techniques can effectively improve the laser damage resistance of optics.

1. Introduction

As a material with excellent optical properties, fused silica is widely used in the fabrication of optics in various high-power laser systems [1], such as NIF in the United States and Laser Megajoule in France [2–4]. When the laser systems operate, a number of induced damages may generate on the optical surface due to strong laser irradiation. The laser damage not only affects the service life of optics but also leads to the distortion of beam line, which can destroy the downstream elements, or even cause irreversible breakdown to the system. In order to tackle the problem, scholars have made some efforts, including improved the growth process of base materials and adopted advanced processing technique [5, 6].

MRF technique is developed by Kordonski in cooperation with the Center for Optics Manufacturing (COM) of Rochester University [7]. The optical materials are removed through high-speed friction between flexible polishing ribbon and surface. The use of flexible polishing ribbon avoids the generation of subsurface damage and is conducive to the improvement of surface quality [8]. Zhao found that MRF can restrain subsurface defects and significantly improve the laser damage resistance of fused silica optics [9]. Based on the theory of magnetorheological elastic polishing, Shu verified experimentally that MRF can achieve nondestructive processing of fused silica optics [10].

As an advanced optical processing technique, IBSE technique is also used to polishing fused silica optics. In IBSE process, high-energy ion beam bombards the surface, and atoms obtain energy and then escape from the surface to achieve materials removal [11]. The noncontact processing model enables IBSE technique not to introduce defects such as pollution and scratches, so as to achieve the goal of manufacturing optical elements with high surface quality and damage threshold. By studying the surface modification, Li found that IBSE can effectively improve the surface state of fused silica, and the damage threshold could reach more than 15 J/cm^2 [12, 13]. Liao detected fused silica surface polished by IBSE technique with high-resolution methods such as atomic force microscope and found that no defects generate on the surface, which proved the effectiveness of the technique [14]. Xu also found that IBSE can reduce the surface roughness and improve the surface quality [15].

In addition to above techniques, AMP has been applied to the post-treatment process of fused silica optics in recent years; for improving laser damage resistance, Bude used AMP 3.0 technique to treat fused silica optics, the defects were obviously passivated, and surface was not damaged under laser irradiation (10 J/cm^2, 351 nm, and 5 ns) [16]. Shao found AMP technique can remove chemical structure defects (ODC/NBOC) introduced in prepolishing process and effectively improve laser damage threshold of fused silica optics [17]. Sun also found AMP can remove Ce or other polluting elements, and the damage threshold of fused silica optics even reached 20 J/cm^2 [18].

Although many scholars have done a lot of work in MRF and IBSE processing of fused silica and confirmed the great advantages of AMP technique in the improvement of damage threshold, there still has little research on the evolution of surface quality and damage characteristics in the combination of above three techniques. Therefore, this work has a certain value.

By means of MRF, IBSE, and AMP technique, this work explored the changes of photothermal absorption and damage density of fused silica optics under different processing parameters. In second part, it introduces the sample preparation, testing, and characterization method. The third part shows the research results. The fourth part discusses the relevant research results, and the fifth part summarizes the work.

2. Materials and Methods

2.1. Sample Preparation. We had prepared 9 pieces fused silica optics made by Likabao Co. Ltd. (size: 100 mm × 100 mm×10 mm, technology: low stress continuous polishing in the same batch, material: Corning 7980, and label: 1#-9#), and sample 1# was applied in slant etching experiment, and samples 2#–7# were applied in ultra-precision machining process. Samples 8# and 9# were used as the contrast, and 8# was a blank control, while 9# was merely treated by AMP technique.

Ultra-Precision Machining Process. Samples 2#–7# were polished by MRF technique to remove the subsurface damage layer first, and then, the optics were polished by IBSE technique with different depths. The parameters of ultra-precision machiningprocessare shown in Tables 1–3.

AMP Process. Samples #2–#7 were processed by AMP technique after MRF and IBSE process. 9# was only etched by AMP technique under the same parameters. The whole AMP process was carried out under the action of Teflon-lined multifrequency ultrasonic transducer (multifrequency ultrasonic frequency: 430 KHz, 1.3 MHz). Firstly, the inorganic acid (70wt.% HNO_3 and 40wt.% H_2O_2, volume ratio 2 : 1) was used for precleaning (time: 80 min), and then, the surface was etched with etchant (70wt.% HF and 30wt.% NH_4F, volume ratio 1 : 4). The etching rate was determined to be 0.1 μm/min. The whole process was carried out in the class 100 clean room. When precleaning and etching steps completed, the surface was cleaned with deionized water. The parameters of etching depth are shown in Table 4.

Table 1: MRF parameters.

Parameters	Value
Flow rate	130 L/h
Electric current	0.8 A
Polishing wheel speed	240r/min
Polishing abrasive	CeO_2
Abrasive diameter	0.2 μm
Volume removal efficiency	3.6×10^7 μm^3/min
Material removal depth	1μm

Table 2: IBSE parameters.

Parameter	Value
Polishing gas	Ar
Angle	0°
Chamber pressure	1×10^{-4} Pa
Removal efficiency	11.5×10^{-3} μm^3/min
Beam energy	900 eV

Table 3: Removal depth of IBSE.

Sample number	Depth (nm)
2#	300
3#	600
4#	900
5#	300
6#	600
7#	900

Table 4: AMP etching depth.

Sample number	Depth (μm)
2#	3
3#	3
4#	3
5#	5
6#	5
7#	5
9#	5

2.2. Surface Profile Test. The surface profile of optic was detected by 6-inch aspheric interferometer (Model: Zygo VerFire Asphere, Zygo Co. Ltd.). The wavefront repeatability RMS of the interferometer was less than 2 nm, and the measurement repeatability RMS was less than 0.05 nm.

2.3. Roughness Test. The roughness of samples was detected by white light interferometer (Zygo Co. Ltd.). The lens multiple was 20x, and the size of single test area was 0.47 mm × 0.35 mm. The test was operated along the pre-calibrated path.

2.4. Photothermal Absorption Test. The photothermal absorption test was carried out on the photothermal absorption platform (ZC Co. Ltd.). The size of detection area was 5 mm × 5 mm, step length was 0.05 mm, pump power was

2W, pulse repetition frequency (PRF) was 50 kHz, integration time was 300 ms, measurement mode was transmission, laser wavelength was 355 nm, and sensitivity of the platform was better than 0.1 ppm.

2.5. Laser Damage Density Test. The laser damage density test was carried out in the Institute of Optoelectronic Technology, Harbin Institute of Technology (test environment is shown in Figure 1). Test wavelength was 355 nm, pulse width (FWHM) was 5 ns, target spot shape was square, spot size was 10 mm × 10 mm (target spot morphology is shown in Figure 2), modulation degree was 2.17, test area was 40 mm × 40 mm (as shown in Figure 3), and single shot interval was 15 min. The test temperature was 20°C ± 0.2°C, and humidity was 35% ± 5%. In laser damage density test, irradiation area of every single pulse did not overlap each other, and the 16 times of irradiated pulse could cover the whole testing area (40 mm × 40 mm).

2.6. Surface Defect Laser Scattering Test. The surface defect laser scattering test was carried out on the laser scattering detection platform (ZC Co. Ltd.), and detection principle is shown in Figure 4. The detection sensitivity was better than 0.5 μm. The size of test area was 40 mm × 40 mm (consistent with the area shown in Figure 3), the temperature was 24°C ± 2°C, and humidity was 40% ± 2%.

3. Result

3.1. Experimental Results of Slant Etching. In this section, slant etching experiment was carried out on sample 1# to determine the depth of subsurface damage layer formed in continuous polishing process, so as to remove it in subsequent process. The slant was etched by IBSE technique, and the surface profile was detected by 6-inch aspheric interferometer, as shown in Figure 5(a).

In slant etching experiment, dwell time of IBSE technique was controlled to form a slant on sample 1# surface. To gasp the effect, a standard line was calibrated on the slant, and the cross-sectional profile is shown in Figure 5(b). The max depth of the slant was 760 nm, and the length was about 80 mm. Then, roughness test was conducted along precalibrated path shown in Figure 5(a). It should be noted that there were two roughness measurement areas corresponding to each depth since the etching slant was symmetric. The roughness value took the average of the two areas, and the results are shown in Figure 6.

In Figure 6, with the increasing of depth, roughness RMS value gradually increased from 1.023 nm at position 1 to 1.589 nm at position 4 and then decreased to 1.120 nm at position 6. According to the results, position 4 had the highest value of roughness and 233 nm might be considered as the approximate depth of damage layer. To determine damage layer depth further, the curve was fitted based on the experiment roughness results.

Through fitting result (Figure 7), the damage layer depth was judged between 233 nm (position 4) and 575 nm (position 5) because of the highest roughness value. However,

Figure 1: Hundred Joule laser test platform.

shallow scratches with depth of several nanometers still appeared at position 5 (Figure 6), which did not meet the inference of damaged layer depth (233<depth<575 nm), and the scratches disappeared at positon 6. Based on roughness fitting curve and the phenomenon occurred at positions 5 and 6, it was considered that damaged layer depth was between 575 nm and 760 nm. In order to avoid the influence of damage layer, the polishing depth of MRF was set to 1 μm to completely remove the damage layer.

3.2. Laser Damage Test Results. In last section, the damage layer depth was preliminarily determined in slant etching experiment, and the damage layer was removed by MRF technique. Then, IBSE and AMP processes were carried out according to the parameters in Tables 3 and 4. Since surface activity was high after AMP process, the damage density was detected with hundred joule laser device first. For each sample, the irradiated laser energy was about 10 J/cm^2, and the laser damage was observed with long focal length microscope.

For sample 8# (blank control), it had the biggest damage density, which was about 0.70625/mm^2, and the damage layer was thought to be the major factor of dense laser-induced damage. The laser damage density of samples 2# and 5# was the smallest among seven samples. The damage density of samples 3# and 4# was equal, which was 0.0025/mm^2. The damage density of sample 6# was about 0.001875/mm^2. The sample 7# had the highest damage density, and about 10 damage points appeared in the test range of 1600 mm^2. From above results, it was considered that damage density was directly related to the removal amount in AMP and IBSE processes. Increasing the removal amount in IBSE process would aggravate the damage density. For AMP process, the larger AMP depth would reduce the damage density, which was contrary to that in IBSE process. As for the result of sample 7#, it would be explained in Discussion.

3.3. Photothermal Absorption Test Results. After laser damage density test, photothermal absorption test was carried out and the results are shown in Figures 8 and 9.

In Figure 8, the average absorption signal of blank control is 0.294 ppm and a few points with high-absorption appeared in the test area, which was link to laser damage points. The result not only represented the absorbed level of

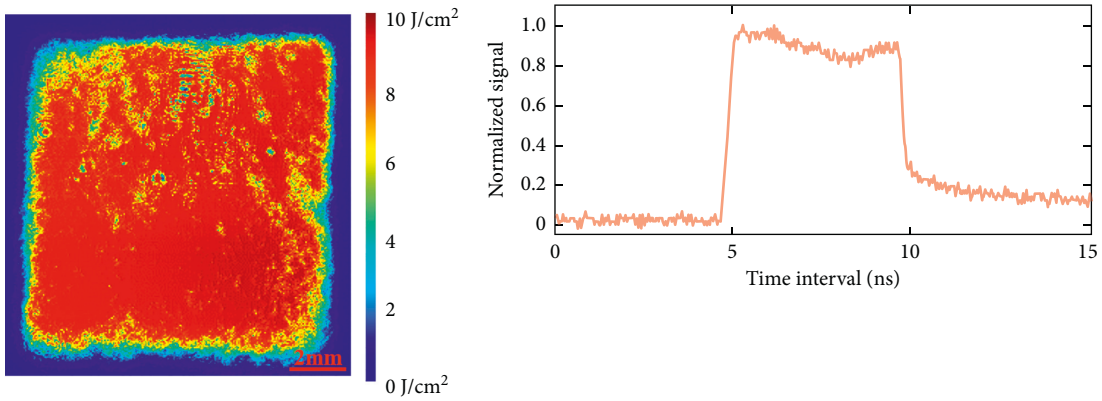

FIGURE 2: Target spot morphology. (a) Target spot (10 mm × 10 mm). (b) Time waveform.

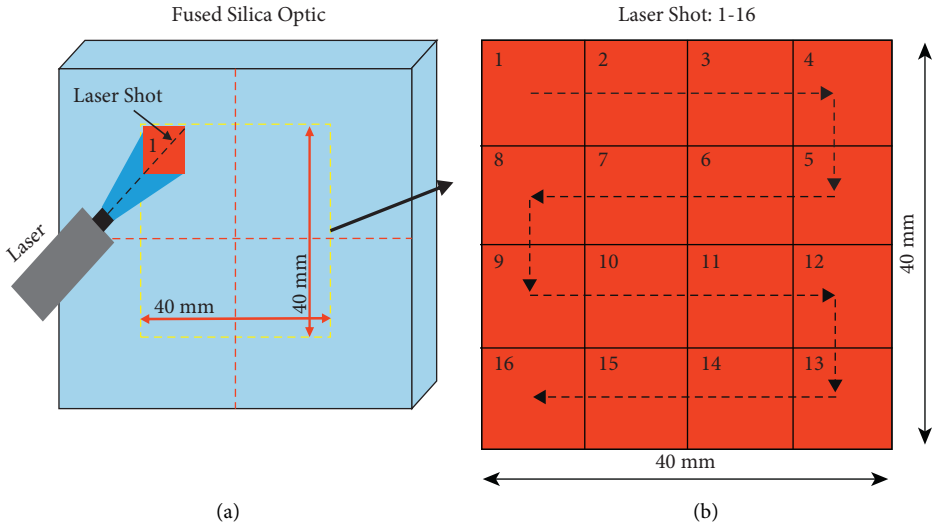

FIGURE 3: Laser damage density test diagram. (a) Test area: 40 mm × 40 mm square area at the center of the surface. (b) Test route: "S"- type route, sequence of laser shots: 1–16.

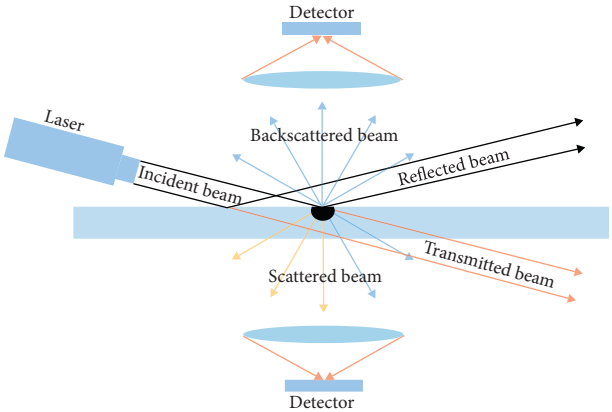

FIGURE 4: Detection principle.

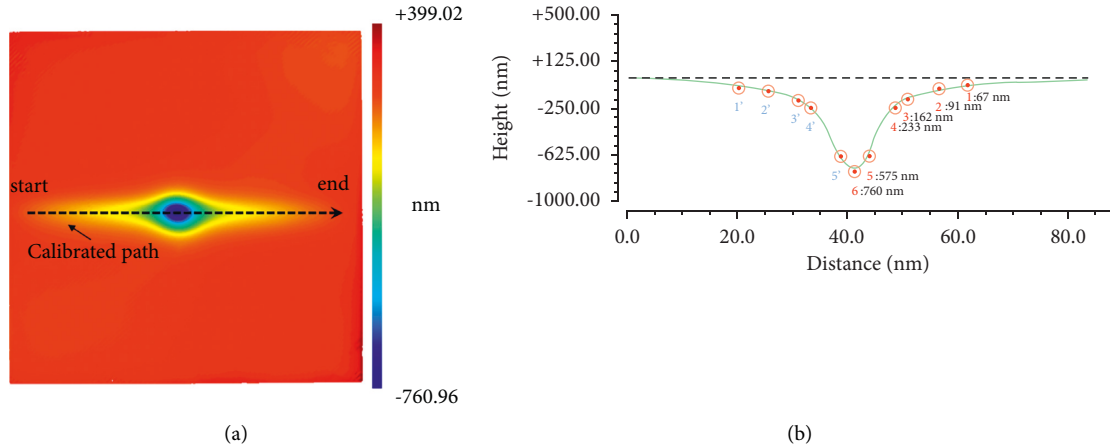

Figure 5: IBSE slant etching results. (a) Slant morphology. (b) Intersecting surface profile.

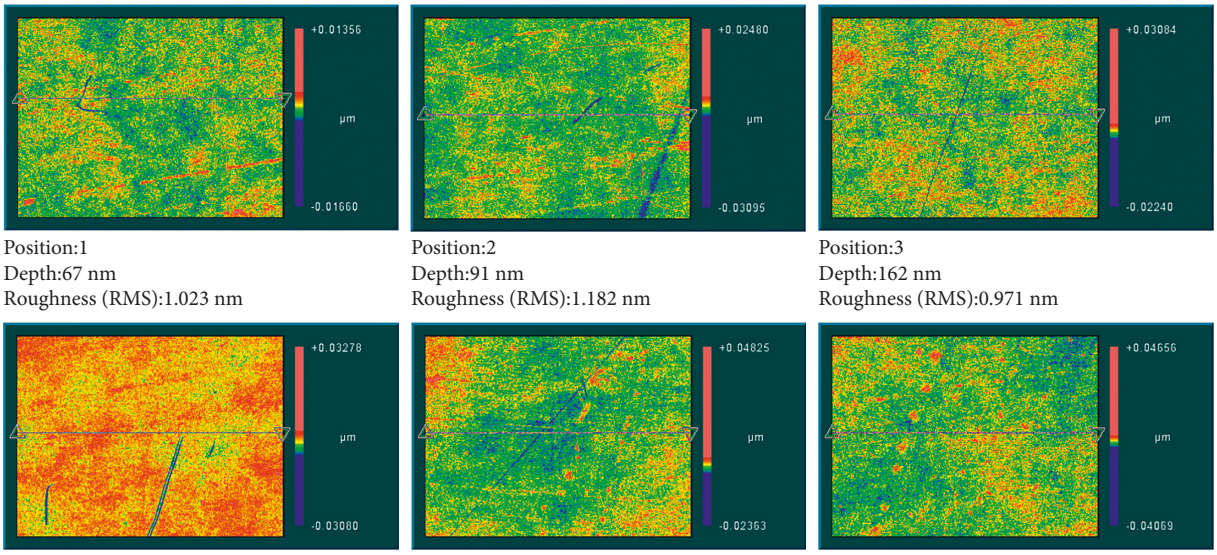

Position:1
Depth:67 nm
Roughness (RMS):1.023 nm

Position:2
Depth:91 nm
Roughness (RMS):1.182 nm

Position:3
Depth:162 nm
Roughness (RMS):0.971 nm

Position:4
Depth:233 nm
Roughness (RMS):1.589 nm

Position:5
Depth:575 nm
Roughness (RMS):1.349 nm

Position:6
Depth:760 nm
Roughness (RMS):1.120 nm

Figure 6: Roughness results.

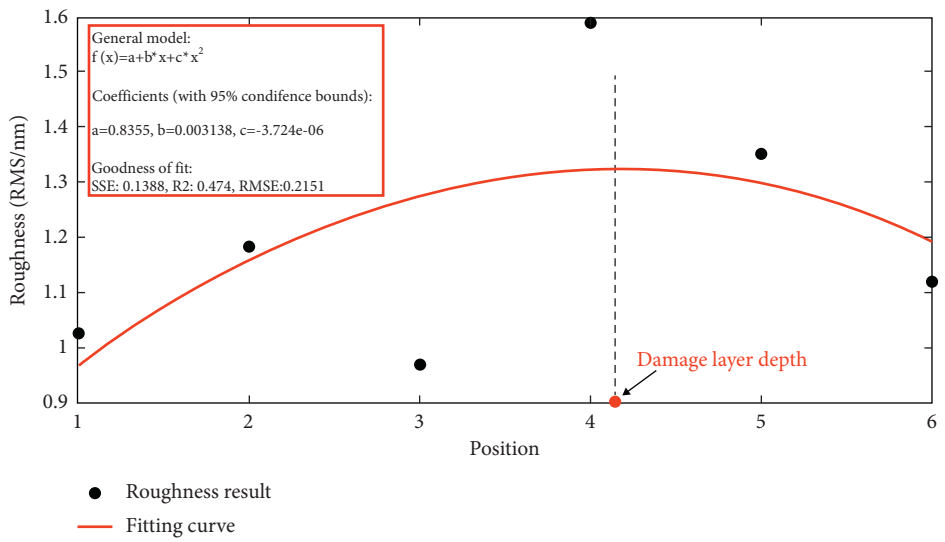

Figure 7: Roughness fitting result.

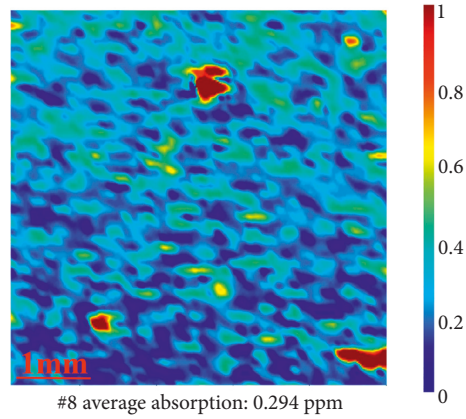

Figure 8: Photothermal absorption result of sample 8#.

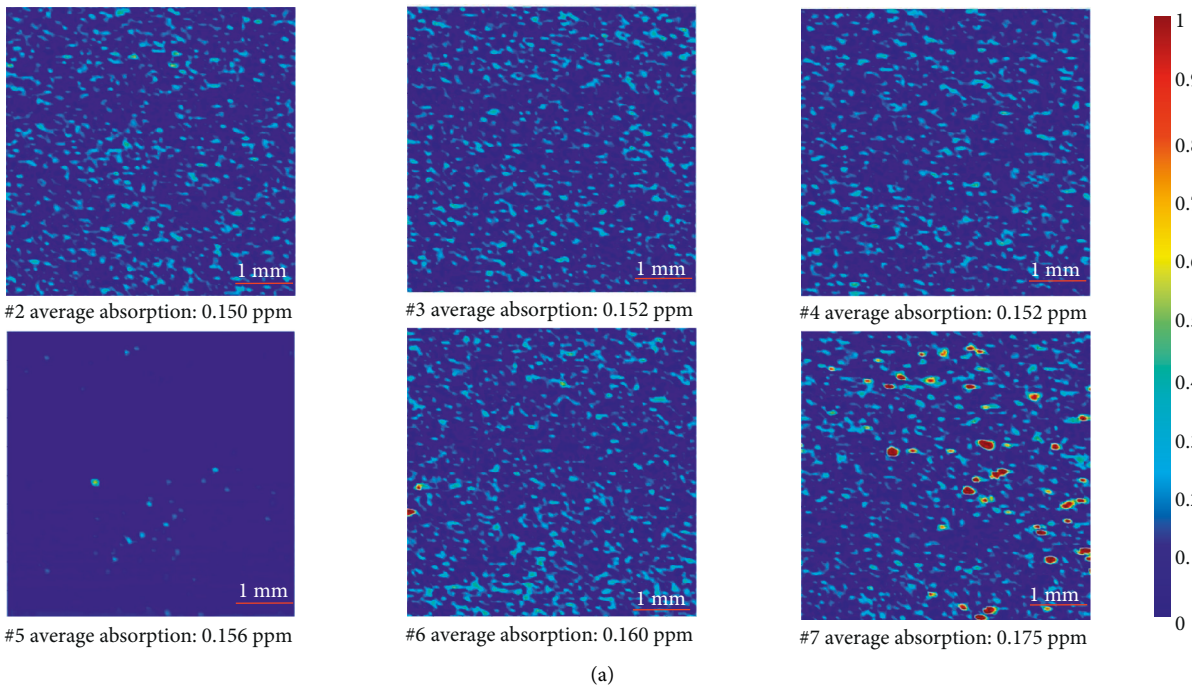

(a)

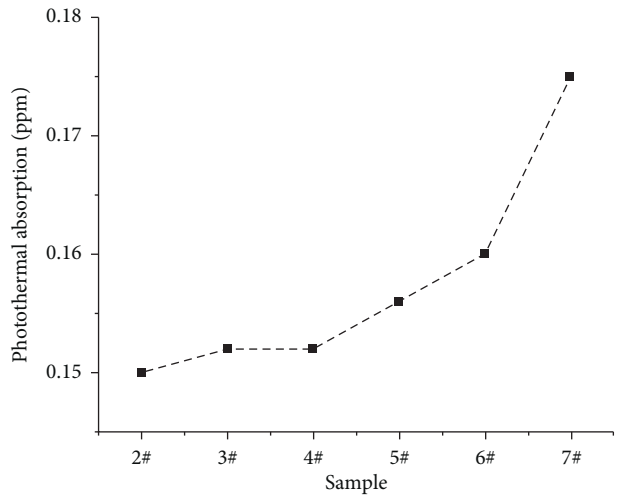

(b)

Figure 9: Photothermal absorption results. (a) Photothermal signal distribution. (b) Photothermal signal evolution curve.

Table 5: Damage density test result.

Sample	Laser energy J/cm^2	Laser shot	Damage spot number	Damage density/mm^2
2#	10	16	2	0.00125
3#	10	16	4	0.0025
4#	10	16	4	0.0025
5#	10	16	2	0.00125
6#	10	16	3	0.001875
7#	10	16	10	0.00625
8#	10	16	1130	0.70625

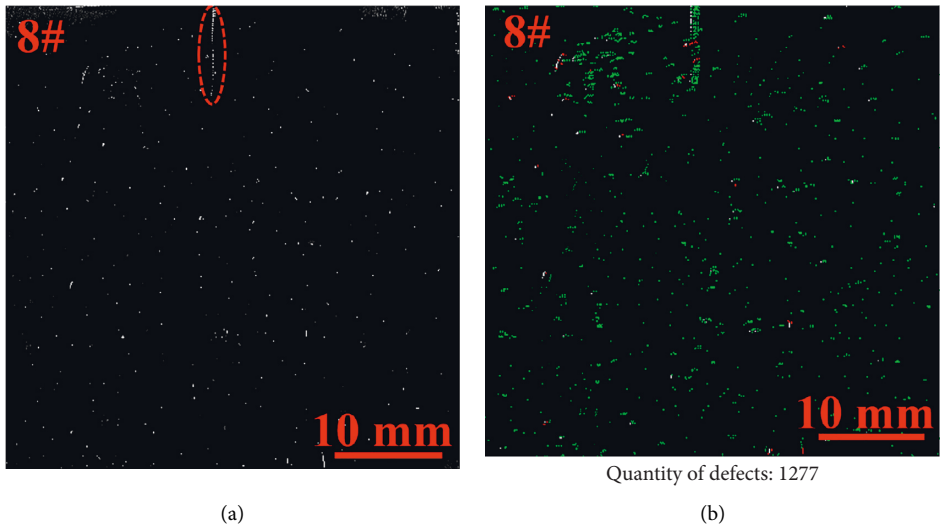

(a) (b)

Figure 10: Laser scattering test results. (a) Dark-field scattering result. (b) Defects identification result.

optics processed in continuous polishing process but also reflected its poor laser damage resistance. For samples 2#–7# (Figure 9), the photothermal absorption signal was 0.150 ppm, 0.152 ppm, 0.152 ppm, 0.156 ppm, 0.160 ppm, and 0.175 ppm, respectively, and the signal levels were significantly lower than that of blank control, which indicated the effectiveness of techniques applied in this work. From Figure 9, it could be seen that the absorption signals of samples 5#, 6#, and 7# were slightly higher than that of samples 2#, 3#, and 4#, which might link to greater AMP etching depth. As for same AMP etching depth, the absorption signal of optics became a little higher as ion beam sputtering depth increased, but basically maintained at the same order. Associated with Table 5, photothermal absorption showed a certain connection with damage density that was the lower absorption signal could bring lower damage density.

3.4. Laser Scattering Detection Results. In this section, sample 8# was detected on laser scattering platform firstly, and the detection area was consistent with that in laser damage density test. The result is shown in Figure 10.

In Figure 10, a large amount of defects appeared on the optical surface after laser irradiation and distributed uniformly. Defects at a few positions also presented aggregation state such as the line type on the top of Figure 10(a). The defects' distribution basically reflected the damage layer formed in low stress continuous polishing process.

In order to grasp the surface conditions of optical surface after IBSE and AMP processes accurately, the defects' distribution of sample 2# to 7# was also detected on laser scattering platform, and the detection areas were also coincided with that in laser damage density test.

In Figure 11(c) and 10(b), it could be seen that the number of surface defects after laser irradiation is larger than that of damage points (Table 5). But, its trend was consistent with the laser damage test results that the more laser damage points generated, the more defects on the optical surface would be identified. From the aspect of IBSE process, the removal depth presented a relationship to defects that was the number of identifiable defects increased along with the increasing of removal depth. As for the aspect of AMP process, it was considered that larger etching depth works on the decrease of defects, and the results of samples 2# to 6# basically proved the viewpoint.

For sample 7#, it should have less defects compared with 4#, but the results went against our expectations, just like the result in laser damage density test. On the surface of sample 7#, a larger amount of defects gathered into one piece and formed a foggy distribution area, even presented no obvious periodic law. On the premise that the sample had been processed by MRF, IBSE, and AMP techniques, it was

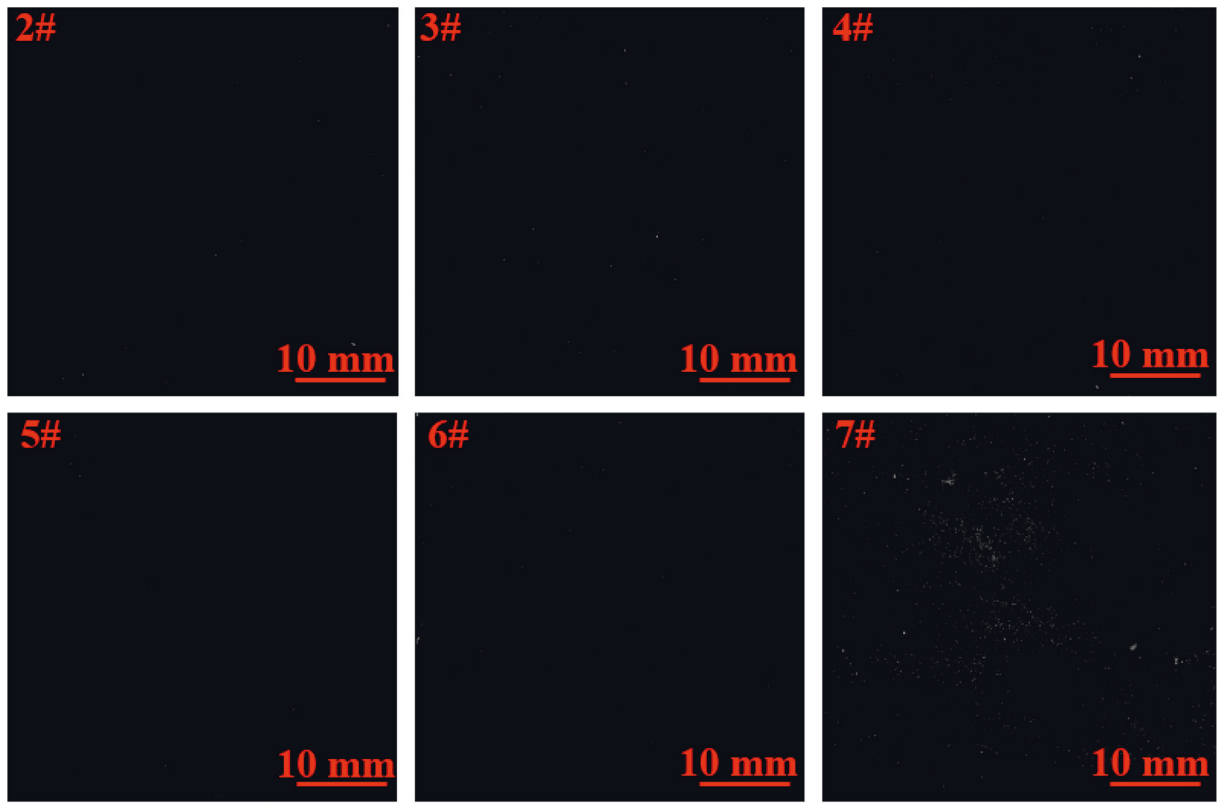

(a)

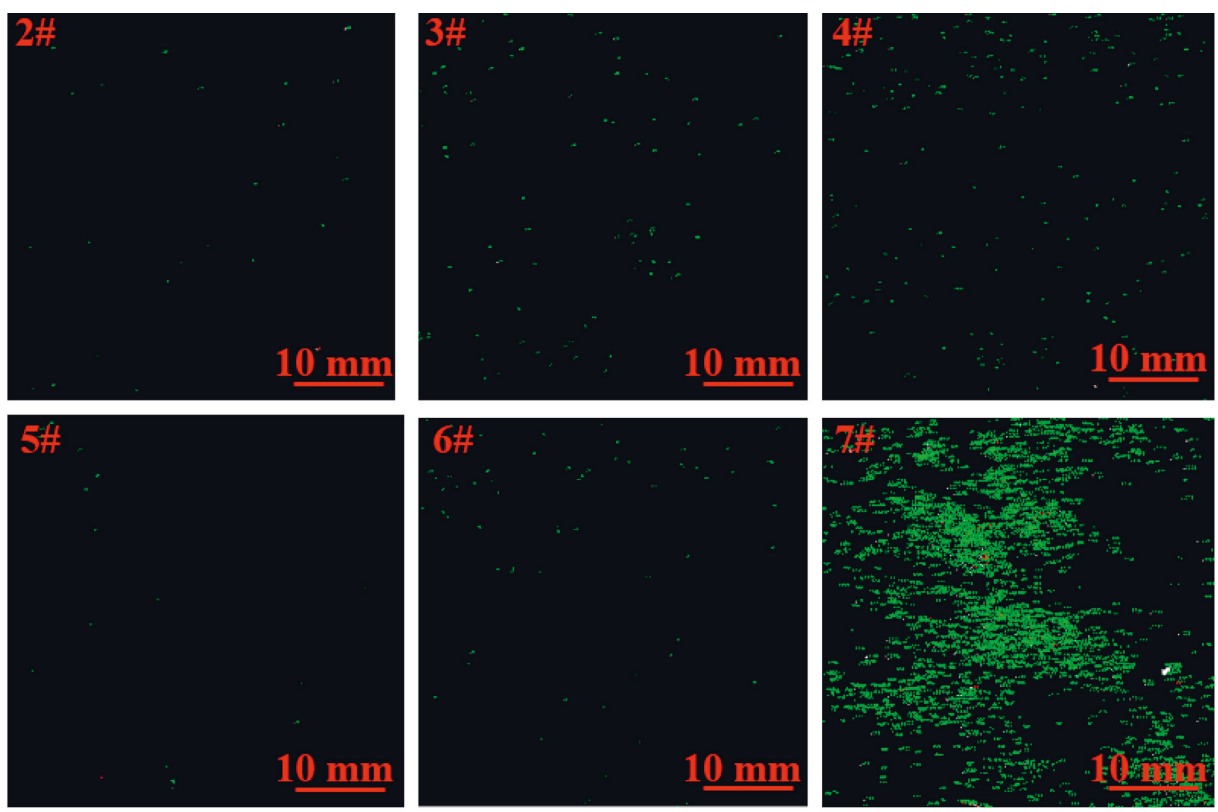

(b)

Figure 11: Continued.

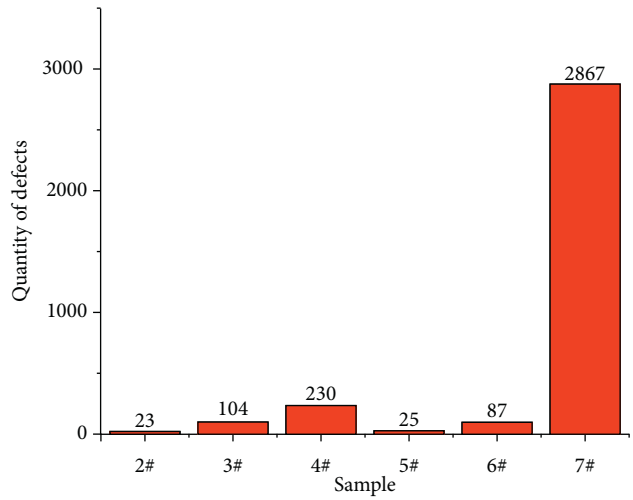

(c)

Figure 11: Laser scattering test results. (a) Dark-field scattering results. (b) Defects identification results. (c) Defects number statistics.

considered that the larger amount of surface defects is related to above techniques. The mechanism will be stated in Discussion.

4. Discussion

Through the experiments in last section, we had a specific acquaintance of laser damage and absorption characteristics of fused silica samples. However, there are still some phenomena worthy of further discussion, and the relevant discussions are stated in this section.

From laser damage density results, it was not difficult to find that deep AMP technique can keep laser damage density maintain at a low level, except sample 7#. Relevant studies pointed out that AMP technique can significantly enhance the laser damage resistance of the optics [19, 20]. Bude even prepared ultra-high-quality surface without damage under 10 J/cm^2 laser irradiation by AMP 3.0 process [16]. For sample 7#, the etching depth of IBSE and AMP was at the maximum, which should have lower damage density. But, the test results were completely contrary to expectation. We speculated that the surface conditions change the damage characteristics. So, the surface morphology of sample 7# was detected by high-resolution microscope equipped in the laser scattering system.

According to the results shown in Figure 12, a large number of massive "fragment" defects appeared on the surface of sample 7# after AMP process. Different from pits, bulges, or other defects, these defects were mainly irregular polygons and attached to the sample surface. After laser irradiation, the typical characteristics of laser damage (as shown in Figure 13) merely appeared in few defects parts, so we think not all "fragment" defects can cause laser damage.

It is always believed that increasing AMP depth can expose purer substrate, optimize the absorption, and damage characteristics. For photothermal absorption results of samples 5#–7#, there were many relatively high-absorption

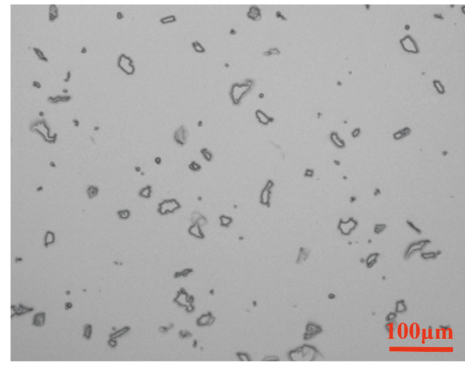

Figure 12: "Fragment" defects.

points, which were more than damage spots generated in damage density test. After comparison, we found the high-absorption points are related to "fragment" defects. Even in the case of "fragment" defects, the average photothermal absorption signal is still maintained at a relatively low level. According to experimental results of sample 7#, "fragment" defects do not strongly affect photothermal absorption, but present a relationship to damage density. When "fragment" defects density is large enough, surface damage characteristics are breakdown, while the absorption level rises a little. For instance, the absorption signal difference of samples 6# and 7# is 0.015 ppm, while the damage density of sample 7# is 3 times of sample 6#. In a conclusion, "fragment" defects with a large amount have great influence on laser damage characteristics, as for absorption characteristics, its effect is relatively less.

As for the formation of "fragment" defects, we initially thought it is caused by AMP technique. Therefore, another piece of fused silica optic (sample 9#) merely etched to 5 μm by AMP technique was detected by laser scattering platform, and foggy "fragment" defects were not found on the surface (Figure 14), which indicated AMP technique is not the major

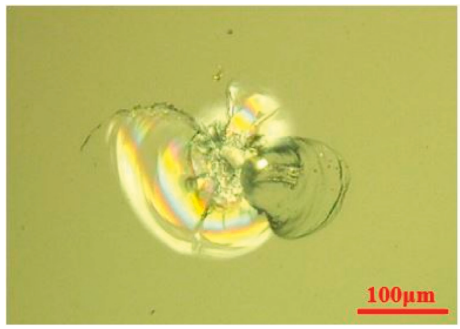

Figure 13: Typical laser-induced damage.

Figure 14: Laser scattering result after AMP etching process.

factor. Through the comparative analysis of two laser scattering figures (sample 7# in Figure 11(b) and sample 9# in Figure 14), we judge that the "fragment" defects must have much to do with MRF or IBSE technique.

For samples 2#–7#, they were all treated by MRF technique to remove materials about 1 μm. After IBSE and AMP process, only the surface of sample 7# generated "fragment" defects, and the results prove that "fragment" defects have nothing to do with MRF technique. Excluding the effects of MRF and AMP technique, IBSE technique is considered to be the major factor.

In our previous study, it had been mentioned that microstructure generates in IBSE process under high beam density or long sputtering time [21] that may affect the AMP etching effect. For AMP technique, its effectiveness in LIDT (laser-induced damage threshold) improvement has already been proved by scholars [17–20] and no special structure has been found under larger etching depth. Combined above statement and the results in this work, we consider that IBSE technique changes the materials characteristics and causes materials densification. In AMP process, dense materials result in the presentation of "fragment" defects, just like sample 7#. We also found a few "fragment" defects appear on the surface of sample 4#, as shown in Figure 15. The discovery proves our inference. For IBSE technique, the removal depth and processing time need to be controlled, limiting the removal amount to about 600 nm. For now, the

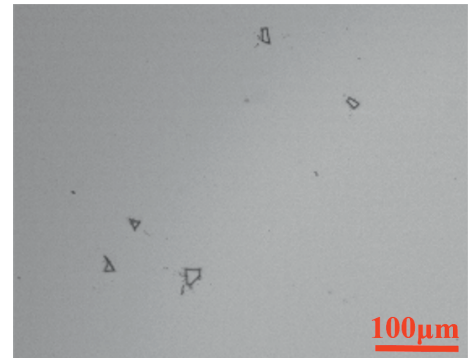

Figure 15: "Fragment" defects of sample 4#.

control of IBSE technical parameters is the priority and in-depth research will be conducted to solve the problem about "fragment" defects in the future work.

For sample 7# with relatively high damage density, we believe that it is not only related to high-density "fragment" defects, but also to SiF_6^- compounds produced in AMP process. This product had been proved to affect the damage threshold of fused silica optics under high-power laser irradiation in relevant studies [22, 23], and this part will also be studied further.

5. Conclusion

Aimed at the increasing requirements of optics applied in high-power laser systems, the authors conducted the research on the manufacture of fused silica by MRF, IBSE, and AMP techniques. Treated by above techniques, not only surface absorption signal maintained at a relatively lower level (about 0.15 ppm) but also damage density decreased in a degree (about 0.00125/mm^2 under 10 J/cm^2 laser irradiation). In general, this work provides a certain function of reference for the fabrication of optics in laser systems. At the same time, some interesting and unknown phenomena occurred in this work, including "fragment" defect. These problems will be settled in further work.

Data Availability

The data used to support the findings of this study can be obtained from the corresponding author upon request.

Conflicts of Interest

The authors declare that they have no conflicts of interest.

Acknowledgments

This work was supported by the National Key R&D Program of China (no. 2020YFB2007504), the National Natural Science Foundation of China (U1801259), Strategic Priority Research Program of the Chinese Academy of Sciences (no. XD25020317), and the National Natural Science Foundation of China (52105495).

References

[1] D. Zhu, Y. Chen, P. Li, B. Feng, and Y. Pang, "Design and management of stray light for compact final optics assembly on the high energy laser system," *International Journal of Optics*, vol. 2021 Article ID 6655866 pp. 1–7, 2021.

[2] P. A. Baisden, L. J. Atherton, R. A. Hawley et al., "Large optics for the national ignition facility," *Fusion Science and Technology*, vol. 69, no. 1, pp. 295–351, 2016.

[3] D. Zhu, P. Li, X. Chai, B. Feng, and Z. Peng, "General design and experiment for separated final optics assembly on high energy laser system," *Optics & Laser Technology*, vol. 128, p. 106213, 2020.

[4] L. Zhang, C. Zhang, J. Chen et al., "Formation and control of bubbles during the mitigation of laser-induced damage on fused silica surface," *Acta Physica Sinica*, vol. 67, no. 1, Article ID 016103, 2018.

[5] M. K. Gupta, D. Dinakar, and I. M. Chhabra, "Experimental investigation and machine parameter optimization for nano finishing of fused silica using magnetorheological," *Optik*, vol. 226, no. 1, 2021.

[6] Z. Cao, C. Y. Wei, X. Cheng et al., "Ground fused silica processed by combined chemical etching and CO2 laser polishing with super-smooth surface and high damage resistance," *Optics Letters*, vol. 45, no. 21, pp. 6014–6017, 2020.

[7] A. Shorey, W. Kordonski, and M. Tricard, "Magneto-rheological finishing of large and lightweight optics," *Proceedings of SPIE*, vol. 5533, pp. 99–107, 2004.

[8] W. Kordonski and S. Gorodkin, "Material removal in magnetorheological finishing of optics," *Applied Optics*, vol. 50, no. 14, pp. 1984–1994, 2011.

[9] Z. Zhao, J. He, Y. Zhang et al., "Evaluation and removal of subsurface damage in polished fused silica by magneto-rheological finishing," *Laser Journal*, vol. 38, no. 7, pp. 13–16, 2017.

[10] Y. Shu, "Study on the Key technique of high-efficiency low-damage fabrication for high-performance ultra-violet laser irradiated fused silica optics," *Doctoral Dissertation*, National University of Defense Technology, 2014.

[11] X. He, C. Cai, H. Zhao et al., "Effect of Ion beam etching on surface/subsurface structural defect evolution in fused silica optics," *Optical Materials*, vol. 116, p. 111096, 2021.

[12] B. Li, *Improvement Laser-Induced Damage Threshold of Fused Silica by Ion Beam Surface Modification*, Doctoral Dissertation, UNIVERSITY OF ELECTRONIC SCIENCE AND TECHNOLOGY OF CHINA, 2019.

[13] B. Li, X. Xiang, W. Liao et al., "Improved laser induced damage thresholds of Ar ion implanted fused silica at different ion fluences," *Applied Surface Science*, vol. 471, pp. 786–794, 2019.

[14] W. Liao, Y. Dai, and X. Xie, "Influence of material removal programming on ion beam figuring of high precision optical surfaces," *Optical Engineering*, vol. 53, no. 9, pp. 095101–095108, 2014.

[15] M. J. Xu, F. Shi, L. Zhou, Y. Dai, X. Peng, and W. Liao, "Investigation of laser-induced damage threshold improvement mechanism during ion beam sputtering of fused silica," *Optics Express*, vol. 25, no. 23, pp. 29260–29271, 2017.

[16] J. Bude, C. W. Carr, P. E. Miller et al., "Particle damage sources for fused silica optics and their mitigation on high energy laser systems," *Optics Express*, vol. 25, no. 10, pp. 11414–11435, 2017.

[17] T. Shao, Z. Shi, L. Sun et al., "Role of each step in the combined treatment of reactive ion etching and dynamic chemical etching for improving the laser-induced damage resistance of fused silica," *Optics Express*, vol. 29, no. 8, pp. 12365–12380, 2021.

[18] L. Sun, T. Shao, J. Xu et al., "Traceless mitigation of laser damage precursors on a fused silica surface by combining reactive ion beam etching with dynamic chemical etching," *RSC Advances*, vol. 8, no. 57, pp. 32417–32422, 2018.

[19] L. Sun, J. Huang, H. Liu et al., "Combination of reaction ion etching and dynamic chemical etching for improving laser damage resistance of fused silica optical surfaces," *Optics Letters*, vol. 41, no. 19, pp. 4464–4467, 2016.

[20] T. Shao, L. Sun, W. Li et al., "Understanding the role of fluorine-containing plasma on optical properties of fused silica optics during the combined process of RIE and DCE," *Optics Express*, vol. 27, no. 16, pp. 23307–23320, 2019.

[21] W. Liao, "Fundamental research on ion beam figuring for sub-nanometer precision optical surfaces," *Doctoral Dissertation*, National University of Defense Technology, 2015.

[22] L. Sun, H. Liu, J. Huang et al., "Reaction ion etching process for improving laser damage resistance of fused silica optical surface," *Optics Express*, vol. 24, no. 1, pp. 199–211, 2016.

[23] Y. Zhong, F. Shi, Ye Tian et al., "Detailed near-surface nanoscale damage precursor measurement and characterization of fused silica optics assisted by ion beam etching," *Optics Express*, vol. 27, no. 8, pp. 10826–10838, 2019.